Journal of ELECTRONIC MATERIALS, Vol. 46, No. 1, 2017
DOI: 10.1007/s11664-016-4872-z

Effect of Ni^{2+} Substitution on the Structural, Magnetic, and Dielectric Properties of Barium Hexagonal Ferrites ($BaFe_{12}O_{19}$)

MUHAMMAD ASIF RAFIQ,[1,2] MOAZ WAQAR,[1] TALHA AHMED MIRZA,[1] AFIFA FAROOQ,[1] and AQIF ZULFIQAR[1]

1.—Department of Metallurgical and Materials Engineering, University of Engineering and Technology, G.T Road, Lahore 54890, Pakistan. 2.—e-mail: asifrafiq@uet.edu.pk

Polycrystalline barium hexaferrites $BaFe_{12-x}Ni_xO_{19}$ ($x = 0$, 0.3 and 0.5) ceramics were synthesized by the conventional solid state route. X-ray diffraction and Fourier transform infrared spectroscopy studies confirmed the successful substitution of Ni in $BaFe_{12}O_{19}$ without the formation of any additional phase. Scanning electron microscopy images showed a platelet-like morphology of particles with an increase of average grain size by the increase in Ni content. A vibrating sample magnetometer revealed that the remnant magnetization M_r and coercivity H_c increased to a large extent, i.e., from 20.24 to 25.51 emu/g and from 1027.20 to 1971.60 Oe, respectively, with the increase in Ni from $x = 0$ to $x = 0.5$; however, saturation magnetization M_s showed a minor variation. Dielectric studies were done using a precision impedance analyzer, which showed a decrease in dielectric loss with the increase in Ni content and very little variation in the conductivity of the samples.

Key words: Barium hexaferrites, conventional solid state route, Ni substitution, magnetic properties, dielectric

INTRODUCTION

Since their discovery more than half a century ago, hexagonal ferrites have received tremendous attention as commercially and technologically important materials. Hexagonal ferrites also known as 'hexaferrites' solely account for more than 50% of the total magnetic materials produced globally[1] owing to their applications in magnetic recording, ferrofluids, sensors, ceramic magnets in loud speakers, electric power generation, rotors in small direct current (DC) motors, automotive electronics, ferrite cores, fabrication of inductors, microelectromechanical systems (MEMS), capacitors, transistors, microwave, and in magnetostatic and electromagnetic devices.[2–4] Among the family of hexaferrites, which includes M, Z, Y, W, X and U-type ferrites, M-Type hexaferrites, especially $BaFe_{12}O_{19}$ has caught the attention of researchers in recent few years owing to their remarkable properties including large coercivity, high magnetocrystalline anisotropy along the c axis, relatively large saturation magnetization, electrical resistivity, low cost, ability to resist corrosion, low eddy current, high Curie temperature and low dielectric losses.[4–8] $BaFe_{12}O_{19}$ has a space group P63/mmc and possesses hexagonal structure resembling that of magnetoplumbite, which is a naturally occurring mineral. A single molecular unit of M-type barium hexaferrites (BaM) comprises four alternating blocks of hexagonally packed (S) and cubically packed (R) layers in a sequence RSR* S* where S* and R* are 180° rotations of S and R, respectively. BaM have lattice parameters $c = 23.17$ Å and $a = 5.89$ Å and have a large c to a ratio (3.94) which is the reason for their large crystalline anisotropy.[1] Fe^{3+} ions are responsible for magnetism in BaM. Each S block has four octahedral Fe^{3+} ions having 4↑ moment and two tetrahedral Fe^{3+} ions having a 2↓, giving a total net moment of 2↑. Similarly, each R block has 3↑ 2↓ octahedral Fe^{3+} ions and 1↑ Fe^{3+} ion at a bipyramidal site giving a total net moment of 2↑. So S + R gives a total moment of 4↑, which equals 20 Bohr magnetrons.[9]

(Received April 27, 2016; accepted August 11, 2016; published online September 12, 2016)

Magnetic applications of BaM can be increased by modifying/improving its magnetic properties including saturation magnetization, remnant magnetization and coercivity, which can be done by substituting Fe^{3+} ions at the crystallographic positions. A literature survey shows that researchers have substituted Fe^{3+} ions by other trivalent ions such as Al^{3+},[2] Ce^{3+},[5] Sm^{3+}[6] or in combination with divalent and tetravalent ions like Mg^{2+}/Ti^{2+},[7] Ni^{+2}/Sn^{+4},[10] Ni^{+2}/Ti^{+4},[10] Ni^{+2}/Zr^{+4},[11] etc. For substitution of a divalent impurity such as Ni^{+2}, Co^{+2}, etc., charge is balanced by vacancies forming in the structure, which may occur at any crystallographic position of Fe^{3+} ions causing modification/improvement of magnetic properties.[12]

Ni is a good candidate for the substitution of Fe in barium hexaferrites due to similar ionic radii and electronic configuration of Ni and Fe.[12] The effect of Ni^{2+} ions on the properties of $BaFe_{12}O_{19}$ has been studied in combination with various tetravalent impurities[10,11,13] which resulted in the enhancement of magnetic and microwave absorbing properties of $BaFe_{12}O_{19}$. In single crystals, addition of Ni^{2+} caused a decrease in saturation magnetization M_s and coercivity H_c.[12] However, little work has been done on the substitution of solely Ni^{2+} in polycrystalline $BaFe_{12}O_{19}$ hexagonal ferrites, which suggests the obvious need of studying the role of Ni^{2+} ions in Ni co-doped $BaFe_{12}O_{19}$. In this work, the effect of Nickel (as a dopant) on the structure, microstructure, magnetic and electrical properties of $BaFe_{12}O_{19}$ has been investigated.

MATERIALS AND METHODS

$BaFe_{12-x}Ni_xO_{19}$ hexaferrites with nickel content x = 0, 0.3 and 0.5 were synthesized by the conventional solid state mixed oxide route. Stoichiometric amounts of pure and dried $BaCO_3$ (Riadel-de Haen, 99%), Fe_2O_3 (UniChem, 99.5%) and NiO (Grey/Green British House Drug Ltd., 99%) were mixed in ethanol for 4 h and then calcined at 900°C in air atmosphere for 5 h. Calcined powder was milled with the aid of ethanol for 3 h. The resulting powders were converted into pellets using a hydraulic press by applying a force of 6000 lb and then sintered at 1300°C for 2 h. Crystallographic properties were studied using an x-ray diffractometer (PANalytical Xpert PRO) with Cu-Kα (λ = 0.154 nm) radiation. Morphology and particle size of the samples were analyzed using a scanning electron microscope (Nova NanoSEM 450). Infrared spectroscopic analysis was done by using Fourier transform infrared (Jasco FT/IR-4100 Spectrometer). Magnetic hysteresis curves were plotted at room temperature by vibrating sample magnetometer [Model: 7407, Lakeshore (USA)]. A precision impedance analyzer (Wayne kerr 6500B) was used to analyze dielectric properties over the frequency range of 1 kHz to 2 MHz at room temperature.

Lattice parameters a and c were calculated according to the formula.[7]

$$\frac{1}{d_{hkl}^2} = \frac{4(h^2 + hk + k^2)}{3a^2} + \frac{l^2}{c^2}, \quad (1)$$

where h, k and l are Miller indices, and d is the interplanar spacing that is determined by Bragg's Law, which is $n\lambda = 2d\sin\theta$. The unit cell volume V_{cell} was calculated from the formula[7]

$$V_{cell} = \frac{\sqrt{3}}{2}a^2c. \quad (2)$$

RESULTS AND DISCUSSION

Figure 1 shows the x-ray diffraction (XRD) patterns of $BaFe_{12-x}Ni_xO_{19}$ with Ni concentration in the order of x = 0, 0.3 and 0.5. XRD patterns confirm the formation of $BaFe_{12}O_{19}$ as a major phase in x = 0. However, an impurity phase was detected, which can be attributed to $BaFeO_{3-x}$. It is already known from the literature that synthesis of monophasic $BaFe_{12}O_{19}$ is very difficult both by conventional and wet chemical methods.[1,14,15] However, it is evident from the XRD patterns for x = 0.3 and x = 0.5 that addition of Ni has suppressed the formation of intermediate phase $BaFeO_{3-x}$ and pure $BaFe_{12}O_{19}$ was obtained. A similar kind of behavior has already been reported in other systems like $BiFeO_3$, where synthesis of monophasic composition was very difficult and dopant suppressed the formation of the second phase and helped to produce single phase multiferroic ceramics.[16] Diffraction peaks are indexed in accordance with Joint Committee on Powder Diffraction Standards (JCPDS) no. 84-0757 for $BaFe_{12}O_{19}$ (Bragg positions are given at the bottom of Fig. 1) and with JCPDS no. 23-1023 for $BaFeO_{3-x}$.

Table I shows the variation in lattice constants by the addition of Ni in $BaFe_{12}O_{19}$ calculated by using MDI JADE software after peak refinement. The secondary phase was neglected to calculate the lattice parameters of primary phase $BaFe_{12}O_{19}$. For pure $BaFe_{12}O_{19}$, the lattice constants are in good agreement with the literature values.[1] As evident from Table I, the lattice parameters of $BaFe_{12}O_{19}$ started to decrease with the increase in the dopant concentration. This behavior of decrease in the lattice parameters has also been observed in Ni doped BaM single crystals prepared by the flux method.[12] At higher substitution rates, apparently the formation of oxygen vacancies (to balance the charge) has a greater effect on lattice parameters as compared to the substitution of Fe^{3+} ions by Ni^{2+} ions in the unit cell, which consequently results in the decrease in lattice parameters.[12]

The room temperature infrared (IR) spectra of sintered samples were recorded in the mid-IR range, 1000–400 cm^{-1}. Figure 2 shows Fourier

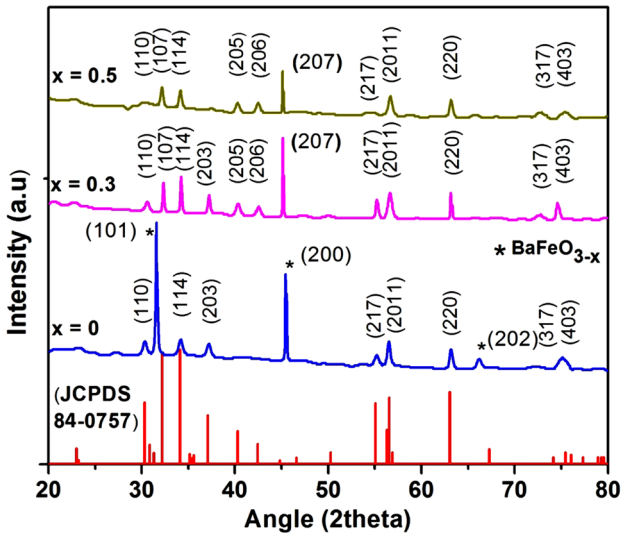

Fig. 1. XRD patterns of $BaFe_{12-x}Ni_xO_{19}$ for $x = 0$, 0.3 and 0.5. Second phase was observed for undoped $BaFe_{12}O_{19}$ whereas addition of Ni suppressed second phase. Bragg peaks for $BaFe_{12}O_{19}$ are present at the bottom for the reference purposes.

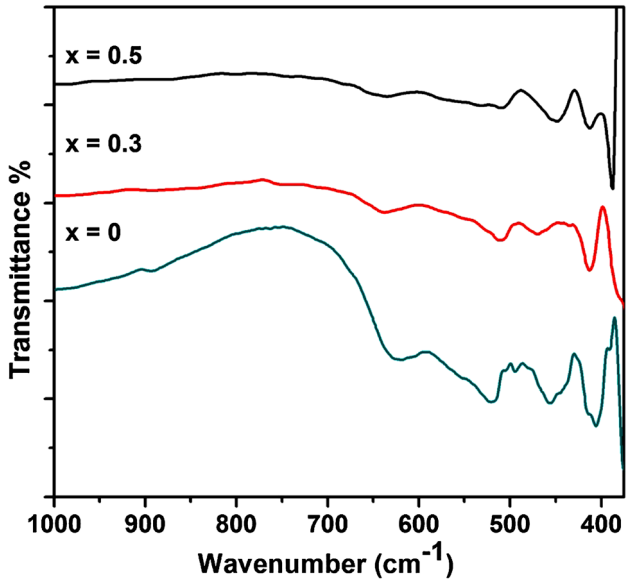

Fig. 2. FTIR spectra of $BaFe_{12-x}Ni_xO_{19}$ for $x = 0$, 0.3 and 0.5. Only metal-oxygen ions were observed indicating the formation of hexaferrites.

Table I. Values of Lattice constant 'a' and 'c', c/a ratio and volume of unit cell of $BaFe_{12-x}Ni_xO_{19}$

x	a (Å)	c (Å)	c/a	V_{cell} (Å)^3
0	5.885	23.260	3.952	697.622
0.3	5.878	23.202	3.947	694.229
0.5	5.873	23.195	3.949	692.839

transform infrared spectroscopy (FTIR) spectra of undoped and doped $BaFe_{12-x}Ni_xO_{19}$ (x = 0.0, 0.3, 0.5). The spectra recorded for all the samples gave two strong characteristic absorption bands in the region between 400 cm^{-1} and 800 cm^{-1}, which are related to the Fe-O stretching and vibration at octahedral and tetrahedral sites. The peaks obtained in the range 550–580 cm^{-1} and 430–470 cm^{-1} were assigned to the vibration of the bond between the oxygen ion and the tetrahedral metal ion (O-M tetra) and octahedral metal ion (O-M octa), respectively.[17] The difference in the peak position was observed in the spectra, which can be attributed to the change in the bond length between Fe^{+3} and O^{-2} ions for tetrahedral and octahedral complexes.[5]

Microstructural analysis was carried out in order to inspect the effect of Ni on grain size and morphology. Figure 3 presents the scanning electron microscopy (SEM) images of $BaFe_{12-x}Ni_xO_{19}$ (x = 0, 0.3, 0.5). Grain size of $BaFe_{12-x}Ni_xO_{19}$ increased with an increase in x, i.e., increase in nickel concentration. Average grain sizes are presented in Table II. From a closer look at the SEM images, large voids among the grains can easily be observed, which might be present due to the oxygen vacancies produced during synthesis at higher temperatures (1300°C). Oxygen vacancies are the most mobile defects, which can easily diffuse and might have played an important role in the grain growth.[16] Morphology of particles is platelet-like for all samples, which is an expected result, keeping in view the anisotropy present in barium hexaferrites as also indicated by the lattice parameters calculated from XRD profiles.

Figure 4 represents the M-H hysteresis curves of the doped and undoped $BaFe_{12-x}Ni_xO_{19}$ (x = 0, 0.3, 0.5) samples measured at room temperature at an external magnetic field of 18.0 kOe. With the addition of Ni, an increase in the coercivity of $BaFe_{12}O_{19}$ was observed as can be seen in Table II. It is well known about barium hexaferrites that their coercivity is related to the uniaxial magnetocrystalline anisotropy along the c axis, and the increase in coercivity (H_c) in this case can be attributed to the enhancement of magnetocrystalline anisotropy by the substitution of Ni^{2+}.[18] Introduction of defects in ceramics is inevitable owing to the fact that they are processed at very high temperatures. It is also known that defects like pores, holes and oxygen vacancies can hinder the movement of magnetic domains and are responsible for the increase in the coercivity. In the present work, increase in defects, especially oxygen vacancies is expected due to the difference in the valency of the substituents, i.e., Fe and Ni which has already been observed in SEM images. This can explain the increase in coercivity in our case and a similar kind of behavior has already been reported for other ceramic systems like $BiFeO_3$ and Potassium-Sodium Niobates.[16,19] Further work is required to fully understand the nature and type of defects. Work in this direction is also being carried out by using impedance spectroscopic

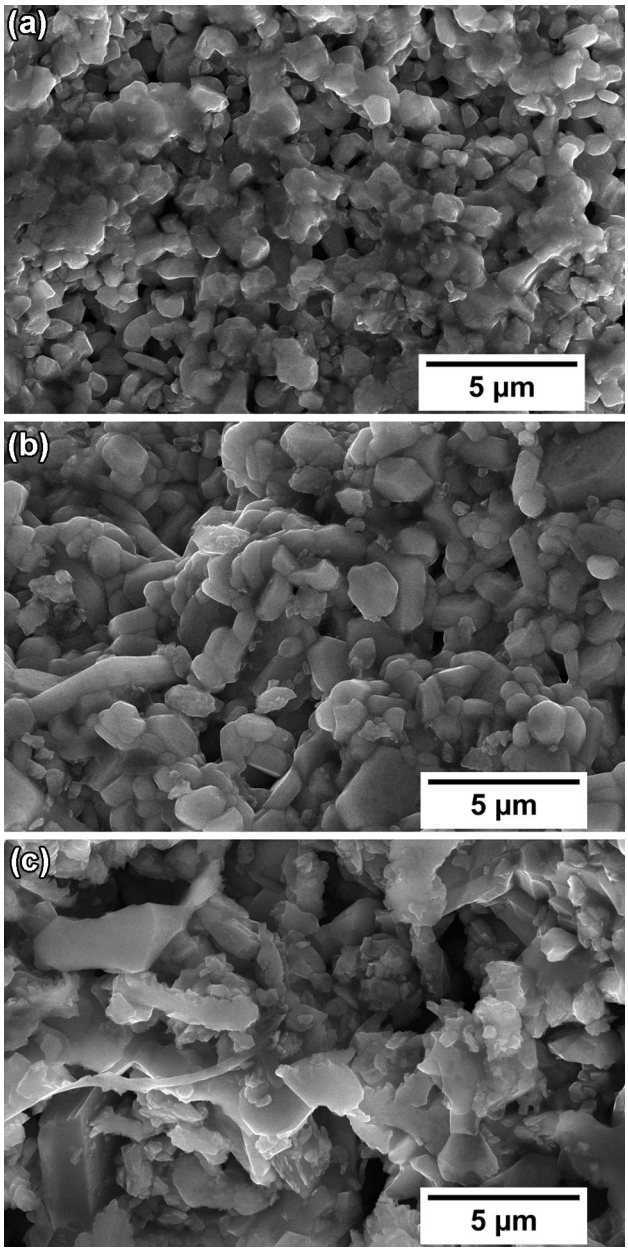

Fig. 3. SEM images of (a) $BaFe_{12}O_{19}$, (b) $BaFe_{11.7}Ni_{0.3}O_{19}$, (c) $BaFe_{11.5}Ni_{0.5}O_{19}$.

techniques and complete results will be published elsewhere.

Remnant magnetization has also increased to a large extent with the increase in Ni concentration. The values of remnant magnetization obtained in our case are comparable with those obtained for nano-sized $BaNi_xCo_{1-x}TiFe_{10}O_{19}$[18] and Pr-Ni substituted $Ca_{0.5}Ba_{0.5}Fe_{12}O_{19}$.[20] Variation of saturation magnetization (M_s) with the increasing amount of Ni^{2+} can be explained by ligand field theory, which states that ions with d^1, d^2, d^3 and d^4 electrons prefer tetrahedral coordination, while ions with d^6, d^7, d^8 and d^9 electrons prefer octahedral coordination. Ni^{+2} ions replace Fe^{+3} ions at $4f_2$ (Spin down) and 12k (Spin up) sites for small values of substitution and prefer 12k (spin up) site for larger amounts. Net magnetic polarization J at temperature T per unit formula of BaM is given by

$$J(T) = 6m_{12k}(T) - 2m_{4f_1}(T) - 2m_{4f_2}(T) + 1m_{2a}(T) + 1m_{2b}(T), \quad (3)$$

where m_n is the magnetic moment of Fe^{3+} ions in the nth sub-lattice.[10] The increase in M_s at $x = 0.3$ suggests that Ni^{2+} ions (3 μ_B) have preferentially replaced Fe^{3+} ions (5μ_B) at $4f^2$ and 12k positions, which resulted in the increase of net magnetic moment. Afterwards, the decrease in M_s at $x = 0.5$ suggest that Ni^{2+} ions substituted Fe^{3+} ions just at the 12k position, which caused a decrease in net magnetic moment. These results are in accordance with the Mössbauer studies of Ni-Zr doped barium hexaferrites.[21] In addition to this, some researchers have also reported this behavior of increasing and decreasing M_s[5,22] and attributed it to the conversion of Fe^{3+} into Fe^{2+} and vice versa as Fe^{2+} has a smaller magnetic moment as compared to Fe^{3+}.

Since dielectric measurements are opening up the space for many specific applications in hexaferrites, therefore, in order to clarify the role of Ni on the dielectric properties we investigated the effect of Ni on permittivity, dielectric loss and conductivity of $BaFe_{12}O_{19}$ at room temperature, i.e., 25°C. The dielectric characteristics of $BaFe_{12-x}Ni_xO_{19}$ over a frequency range 1 kHz to 2 MHz are shown in

Table II. Magnetic properties and average grain size of $BaFe_{12-x}Ni_xO_{19}$ for x = 0, 0.3 and 0.5

X	Saturation magnetization M_s (emu/g)	Remanent magnetization M_r (emu/g)	Coercivity H_c (Oe)	Average size (μm)
0	55.35	20.24	1027.2	0.9723
0.3	57.57	20.65	1240.6	1.4147
0.5	56.42	25.51	1971.6	1.9005

Increase in the remanent magnetization was observed by the increase of Ni content.

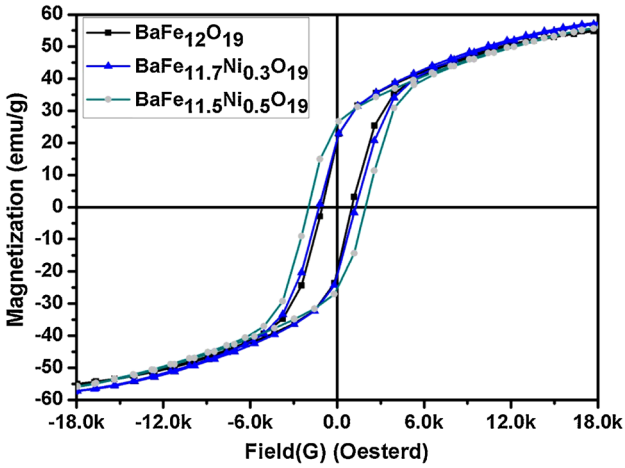

Fig. 4. M-H loop for $BaFe_{12-x}NixO_{19}$ for x = 0, 0.3 and 0.5. Remnant magnetization and coercivity both increased by increasing the Ni content.

Fig. 5. The variation of the real and imaginary part of complex permittivity (ε' and ε'') over a frequency range of 1 kHz to 2 MHz for samples of $BaFe_{12-x}Ni_xO_{19}$, where x = 0, 0.3 and 0.5, is shown in Fig. 5a and b. The real part of the complex permittivity (ε') represents the quantity of stored energy in the dielectric material from the alternating current (AC) field and the imaginary part (ε'') represents the losses.[23] The real part ε' of complex permittivity showed a decreasing trend with the increasing frequency for all the samples over the measured frequency range. There was a decrease in ε' for substitution amount $x = 0.3$, which then increased by increasing the amount of Ni to $x = 0.5$. The imaginary part ε'' of complex permittivity showed a decreasing trend with the increase in frequency except for the sample $BaFe_{11.5}Ni_{0.5}O_{19}$, which showed an increase in ε'' at higher frequencies.

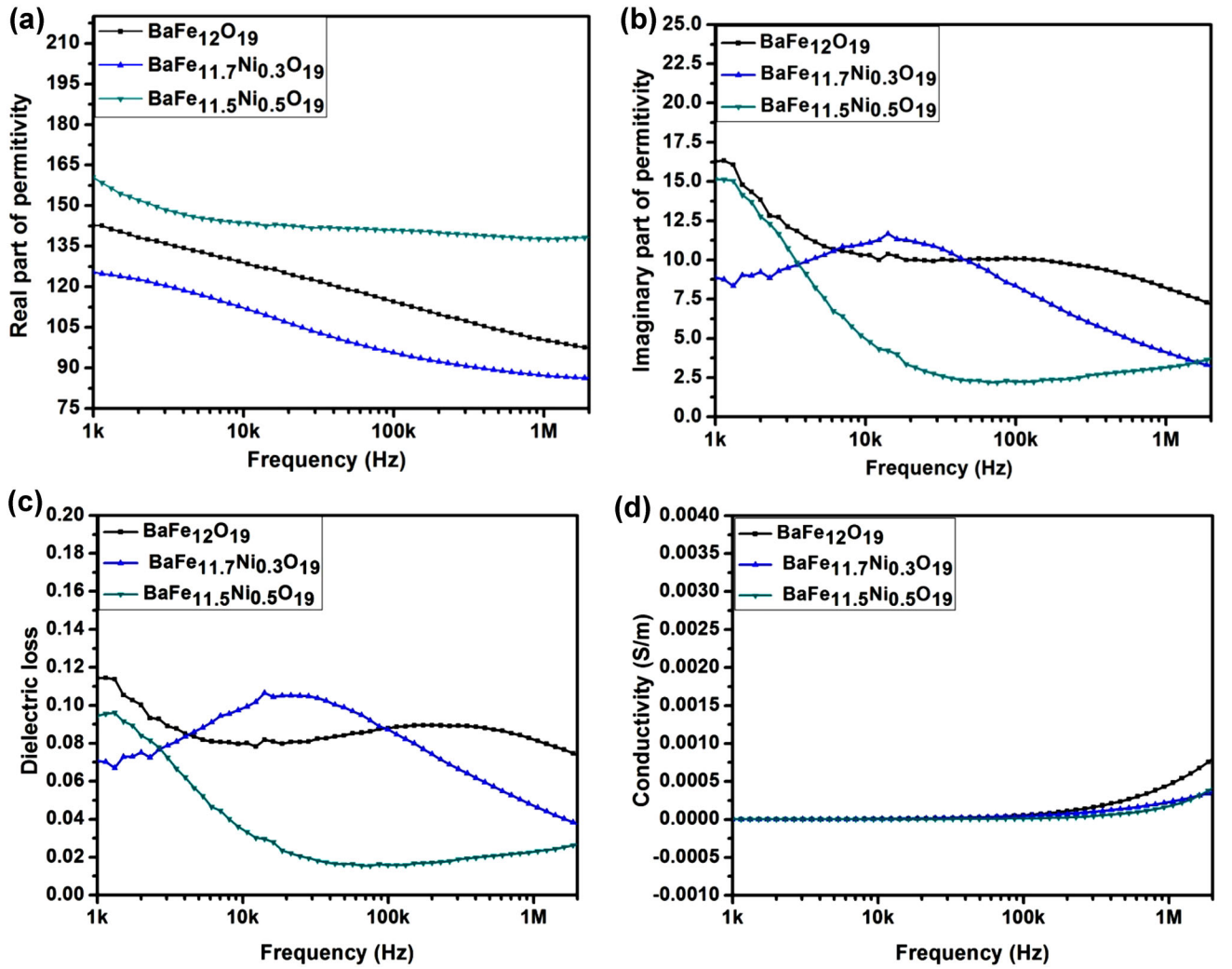

Fig. 5. Effect of frequency on a (a) real part of permittivity, (b) imaginary part of permittivity, (c) dielectric loss and (d) conductivity of $BaFe_{12-x}Ni_xO_{19}$ for x = 0, 0.3, and 0.5.

Figure 5c shows the variation of dielectric loss (tan δ) with frequency for samples $x = 0$, 0.3, 0.5. Dielectric loss remained nearly constant for the sample $BaFe_{12}O_{19}$ over the measured frequency range. For $BaFe_{11.7}Ni_{0.3}O_{19}$, dielectric loss increased at the mid-frequency range and then started decreasing at higher frequency. However, a large drop in the dielectric loss was observed for the sample $BaFe_{11.5}Ni_{0.5}O_{19}$ with increasing frequency. The value of dielectric loss varied between 0.015 to 0.11 for all the compositions. A decrease in dielectric loss was observed with the increasing amount of dopant. Dielectric loss as low as 0.0154 was obtained at a frequency of 75298.7 Hz for sample $BaFe_{11.5}Ni_{0.5}O_{19}$. Figure 5d shows the effect of frequency and the amount of dopant on the conductivity of $BaFe_{12-x}Ni_xO_{19}$. The conductivity of the samples remained approximately unchanged at lower frequency, but at higher frequency, a slight increase in conductivity was observed. The mechanism of conduction in hexaferrites is explained by the hopping mechanism of charge carriers between the Fe ions at octahedral sites. The increase in conductivity at higher frequency is attributed to the increased mobility of charge carriers. At lower frequency, grain boundaries are active, posing high resistance to charge carriers, which explains the low conductivity at lower frequency. At higher frequency, grains tend to be active resulting in a decrease in resistance and, moreover, there is an increase in electrons hopping among Fe^{3+} and Fe^{2+} ions, which is attributed to the increase in the conductivity at higher frequency.[24,25] Further work is required to fully understand this mechanism and work in this direction is also being carried out by using the impedance spectroscopic technique and complete results will be published elsewhere.

CONCLUSIONS

Ni-substituted barium hexaferrite samples have been successfully synthesized using the solid state mixed oxide route. X-ray diffraction reveals the formation of an impurity phase in pure $BaFe_{12}O_{19}$ samples, which is eliminated by the addition of Ni. SEM analysis shows the anisotropy by having platelet-like morphology of the particles, and the average particle size increases with the increase of Ni addition. Coercivity H_c and remnant magnetization M_r increase from 1027.20 to 1971.60 Oe and from 20.24 emu/g to 25.51 emu/g, respectively, with the addition of Ni from $x = 0$ to $x = 0.5$. A dielectric study shows that the dielectric loss of $BaFe_{12}O_{19}$ decreases with the increase in Ni content, whereas conductivity remains almost unaffected.

REFERENCES

1. R.C. Pullar, *Prog. Mater. Sci.* 57, 1191 (2012).
2. D. Chen, I. Harward, J. Baptist, S. Goldman, and Z. Celinski, *J. Magn. Magn. Mater.* 395, 350 (2015).
3. X. Niu, X. Liu, S. Feng, F. Lv, F. Huang, X. Huang, Y. Ma, and K. Huang, *Optik* 126, 5513 (2015).
4. G.M. Rai, M. Iqbal, and K. Kubra, *J. Alloys Compd.* 495, 229 (2010).
5. Z. Mosleh, P. Kameli, A. Poorbaferani, M. Ranjbar, and H. Salamati, *J. Magn. Magn. Mater.* 397, 101 (2016).
6. L. Wang, J. Zhang, Q. Zhang, N. Xu, and J. Song, *J. Magn. Magn. Mater.* 377, 362 (2015).
7. M.H. Shams, A.S. Rozatian, M.H. Yousefi, J. Valíček, and V. Šepelák, *J. Magn. Magn. Mater.* 399, 10 (2016).
8. V.N. Dhage, M. Mane, A. Keche, C. Birajdar, and K. Jadhav, *Phys. B* 406, 789 (2011).
9. J. Smit and H.P.J. Wijn, *Ferrites* (Eindhoven: N.V Philips Gloeilampenfabrieken, 1959), pp. 139–142.
10. H. Sözeri, H. Deligöz, H. Kavas, and A. Baykal, *Ceram. Int.* 40, 8645 (2014).
11. M.V. Rane, D. Bahadur, S. Kulkarni, and S. Date, *J. Magn. Magn. Mater.* 195, L256 (1999).
12. D. Vinnik, D. Zherebtsov, L. Mashkovtseva, S. Nemrava, A. Semisalova, D. Galimov, S. Gudkova, I. Chumanov, L. Isaenko, and R. Niewa, *J. Alloys Compd.* 628, 480 (2015).
13. A. Gonzalez-Angeles, G. Mendoza-Suárez, A. Gruskova, I. Toth, V. Jančárik, M. Papanova, and J. Escalante-Garcı, *J. Magn. Magn. Mater.* 270, 77 (2004).
14. V. Sankaranarayanan and D. Khan, *J. Magn. Magn. Mater.* 153, 337 (1996).
15. K.S. Moghaddam and A. Ataie, *J. Alloys Compd.* 426, 415 (2006).
16. I. Coondoo, N. Panwar, M.A. Rafiq, V.S. Puli, M.N. Rafiq, and R.S. Katiyar, *Ceram. Int.* 40, 9895 (2014).
17. V.C. Chavan, S.E. Shirsath, M.L. Mane, R.H. Kadam, and S.S. More, *J. Magn. Magn. Mater.* 398, 32 (2016).
18. P. Meng, K. Xiong, L. Wang, S. Li, Y. Cheng, and G. Xu, *J. Alloys Compd.* 628, 75 (2015).
19. M.A. Rafiq, A. Tkach, M.E. Costa, and P.M. Vilarinho, *PCCP* 17, 24403 (2015).
20. H.M. Khan, M. Islam, Y. Xu, M.N. Ashiq, I. Ali, M.A. Iqbal, and M. Ishaque, *Ceram. Int.* 40, 6487 (2014).
21. M.V. Rane, D. Bahadur, A. Nigam, and C. Srivastava, *J. Magn. Magn. Mater.* 192, 288 (1999).
22. B. Rai, S. Mishra, V. Nguyen, and J. Liu, *J. Alloys Compd.* 550, 198 (2013).
23. P. Shepherd, K.K. Mallick, and R.J. Green, *J. Magn. Magn. Mater.* 311, 683 (2007).
24. S. El-Sayed, T. Meaz, M. Amer, and H. El Shersaby, *Phys. B* 426, 137 (2013).
25. V.V. Soman, V. Nanoti, and D. Kulkarni, *Ceram. Int.* 39, 5713 (2013).